Supplemental Figure 1

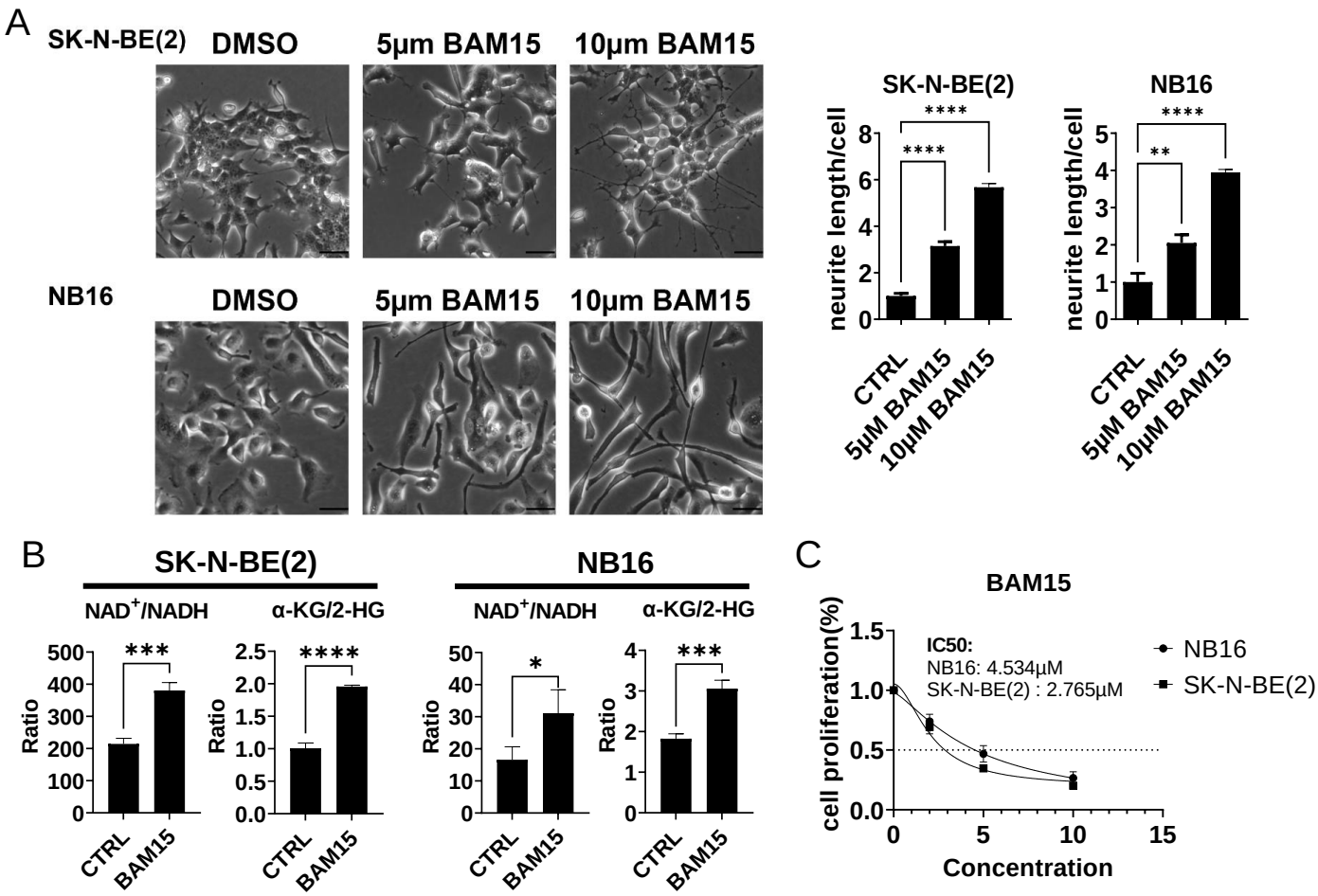

Supplemental Figure 1. Mitochondrial uncoupling is essential for inducing cell differentiation in neuroblastoma.
(A) Left: morphological feature of SK-N-BE(2) and NB16 cells treated with DMSO, 5μM or 10μM BAM15 for 96h (Scale bar: 50 μM). Right: Quantification of neurite outgrowth with NeuronJ. **(B)** Relative cellular NAD^+/NADH and α-KG/2-HG ratio were measured using LC-MS in SK-N-BE(2) and NB16 cells treated with DMSO or 5μM BAM15 for 5h. **(C)** Cells were plated in 12 wells plates ($2x10^4$ cells/well). After 24hrs, cells were treated with DMSO or different concentration of BAM15 for 3 days, and then counted. All the cell numbers were normalized to the control group. In **(A) (B)**, data are represented as mean ± SD of three biological repeats. *P < 0.05; **P <0.01; ***P < 0.001, ****P < 0.0001, determined by Student's two-tailed t-test or One-Way ANOVA test.

Supplemental Figure 2

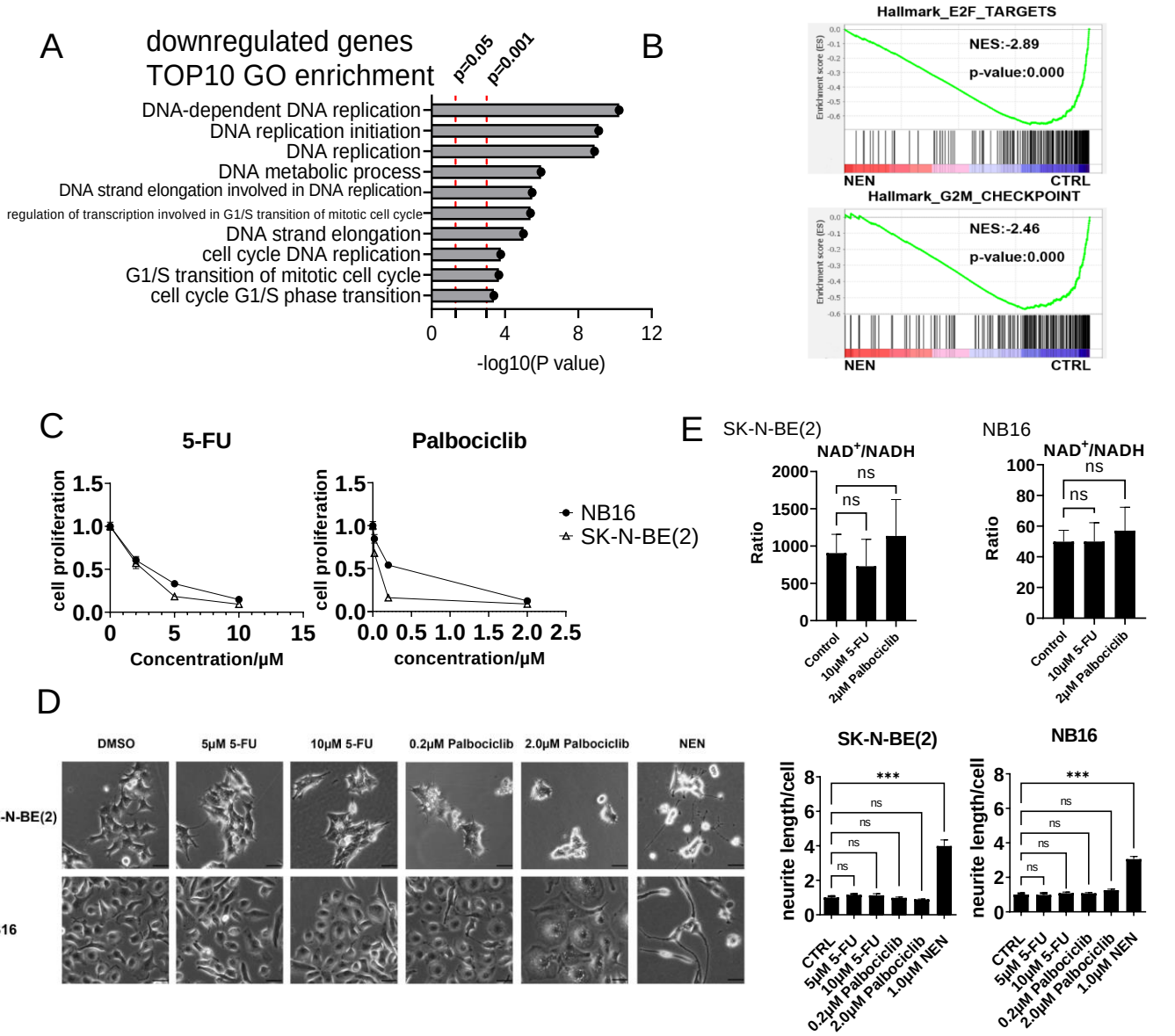

Supplemental Figure 2. Cell cycle inhibitors do not induce cell differentiation in neuroblastoma.
(A) The top 10 GO pathways enrichment of NEN-downregulated genes using DAVID analysis. (**B**) GSEA of E2F targets and G2M checkpoints pathway genes from the RNA-seq experiment in Figure 1**. (C)** Cells were treated with DMSO or different concentration of Fluorouracil(5-FU) or Palbociclib for 3 days, and then counted. All the cell numbers were normalized to the control group. **(D)** Left: morphological feature of cells treated with DMSO or indicated concentrations of 5-FU or Palbociclib for 96h (Scale bar: 50 μM). Right: Quantification of neurite outgrowth with NeuronJ. **(E)** Relative cellular NAD^+/NADH ratio were measured using LC-MS in cells treated with DMSO,10μM 5-FU or 2μM Palbociclib for 5h. Data in **(C) (D) (E)** are presented as mean ± SD of three biological repeats. *P < 0.05; **P <0.01; ***P < 0.001, ****P < 0.0001, determined by One-Way ANOVA test.

Supplemental Figure 3

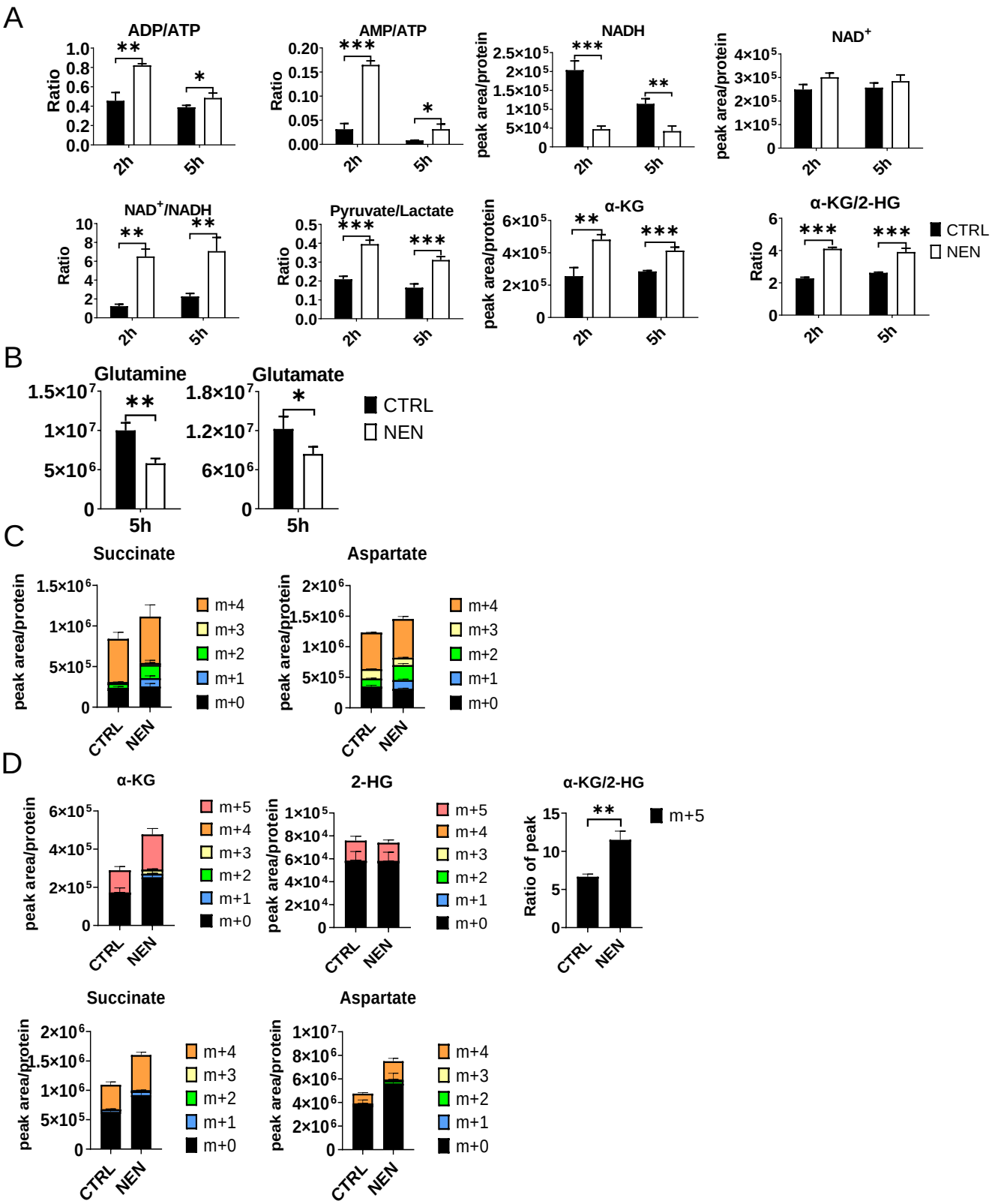

Supplemental Figure 3. NEN treatment increases NAD$^+$/NADH ratio and α-KG/2-HG ratio.

(A) Relative cellular metabolite levels were measured using LC-MS in NB16 cells treated with DMSO or 1 μM NEN for 2h or 5h. **(B)** Relative cellular L-glutamine and L-glutamate levels were measured using LC-MS in NB16 cells treated with DMSO or 1 μM NEN for 5h. **(C)** SK-N-BE(2) and **(D)** NB16 and cells were pretreated by DMSO or 1 μM NEN for 3h, then labeled with U-^{13}C-glutamine for 2h. Relative isotopic labelling abundance in α-KG, 2-HG, succinate, asparate and the ratio of m+5 α-KG/m+5 2-HG were measured using LC-MS. Data were presented as mean ± SD of three biological replicates. *P < 0.05, **P < 0.01, ***P < 0.001, determined by the Student two-tailed t test.

Supplemental Figure 4

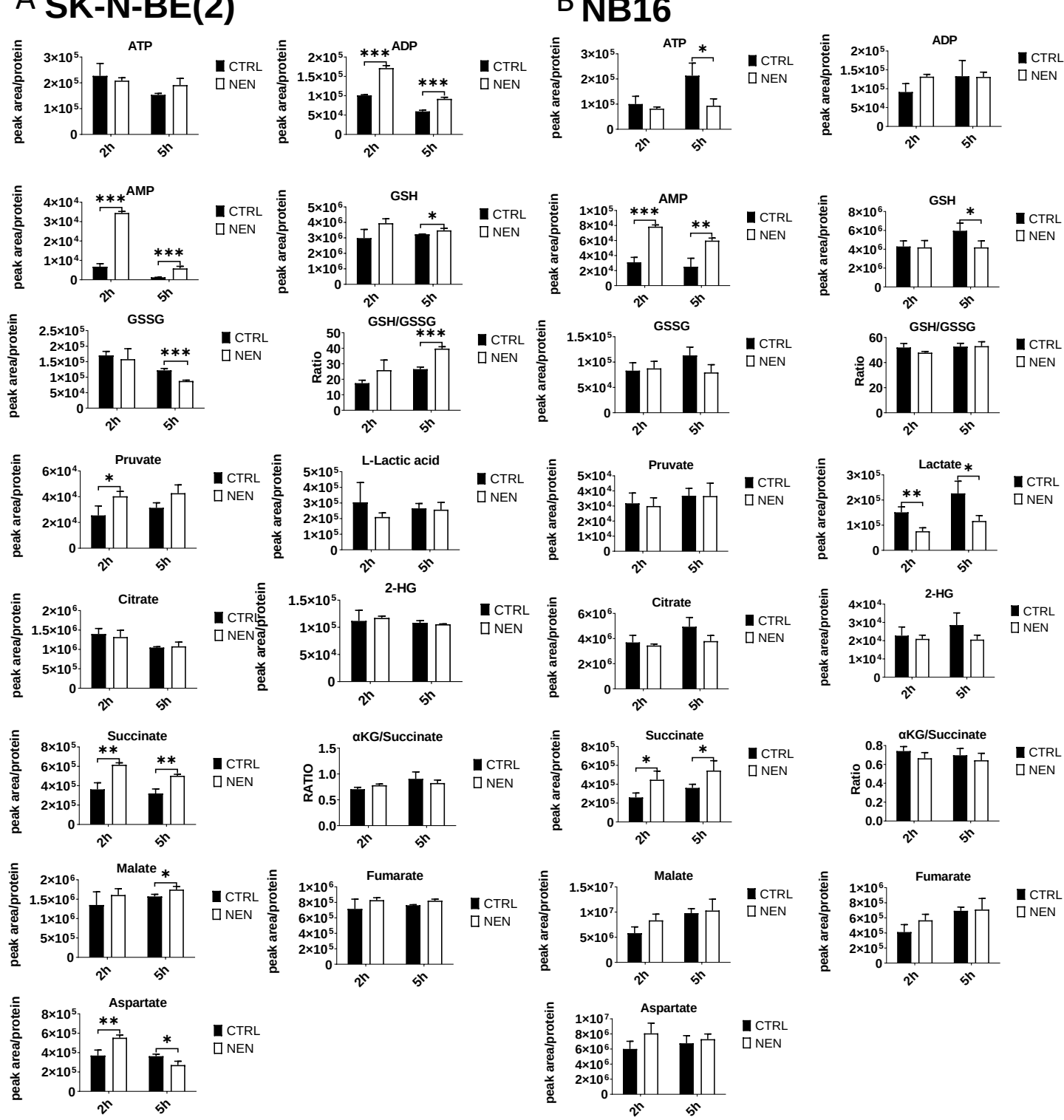

Supplemental Figure 4. The metabolic changes upon NEN treatment.
(A), (B) relative intracellular metabolite levels in the same samples in Figure **2A** and **Supplemental Figure 3A** . Data represent mean ± SD (n = 3, biologically repeats). Representative of at least two independent experiments was shown. *P < 0.05, **P < 0.01, ***P < 0.001, determined by the Student two-tailed t test.

Supplemental Figure 5

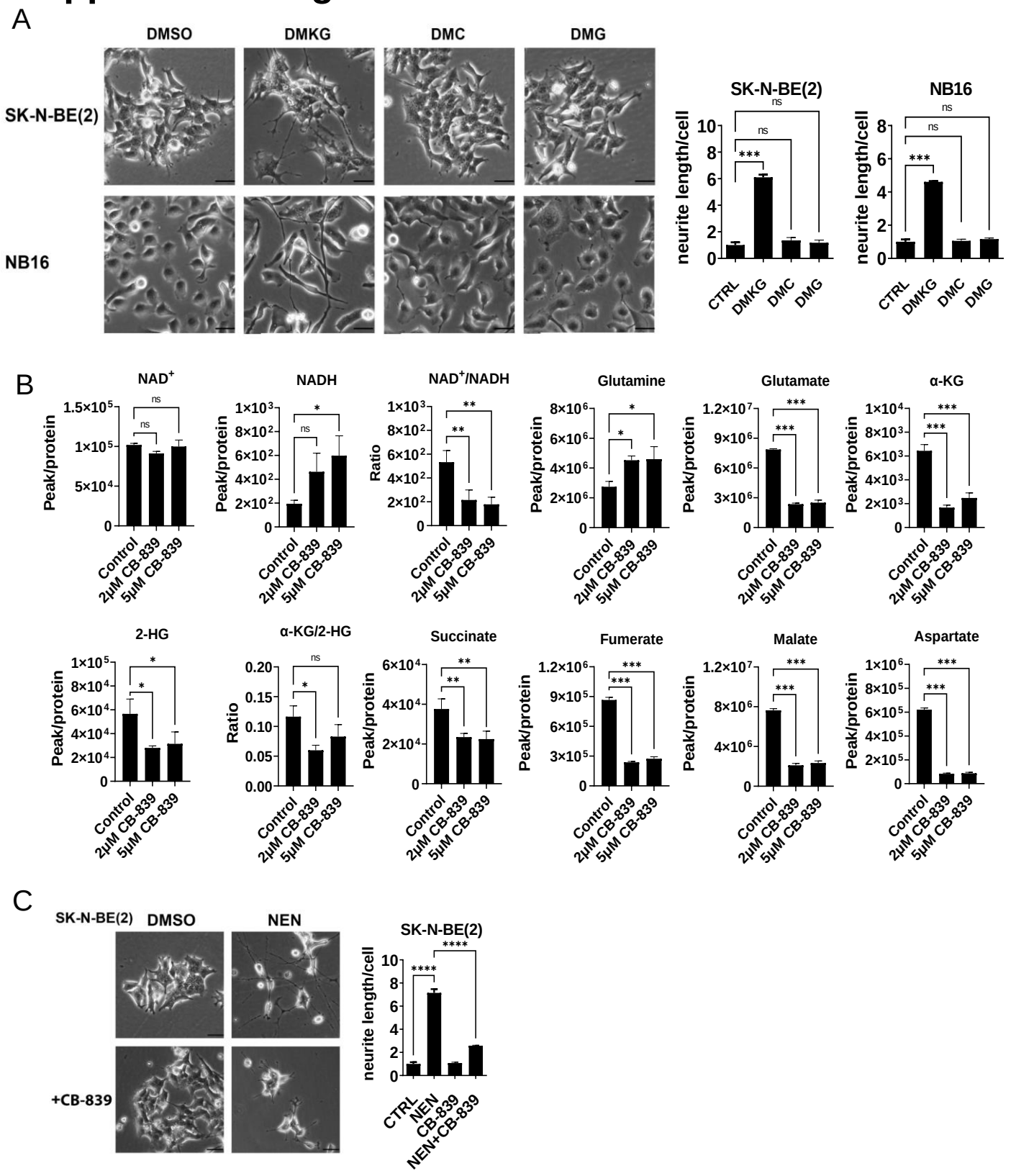

Supplemental Figure 5. α-KG derived from glutaminolysis is necessary for NEN-induced neuroblastoma cell differentiation.

(A) Left: morphological feature of SK-N-BE(2) and NB16 cells treated by 3.5mM dimethyl 2-oxoglutarate (DMKG) or dimethyl carbonate (DMC) or dimethyl glutarate (DMG) for 96h (Scale bar: 50 μM). Right: Quantification of neurite outgrowth with NeuronJ. **(B)** Relative intracellular metabolites were measured using LC-MS in SK-N-BE(2) cells treated with DMSO or 2μM or 5μM CB-839 for 5h. **(C)** Left: morphological feature of SK-N-BE(2) and NB16 cells treated by 1μM NEN with or without 2μM CB-839 for 96h (Scale bar: 50 μM). Right: Quantification of neurite outgrowth with NeuronJ. Data is represented as mean ± SD of three biological repeats. ns: P > 0.05, *P < 0.05; **P <0.01; ***P < 0.001, ****P < 0.0001, determined by One-Way ANOVA test.

Supplemental Figure 6

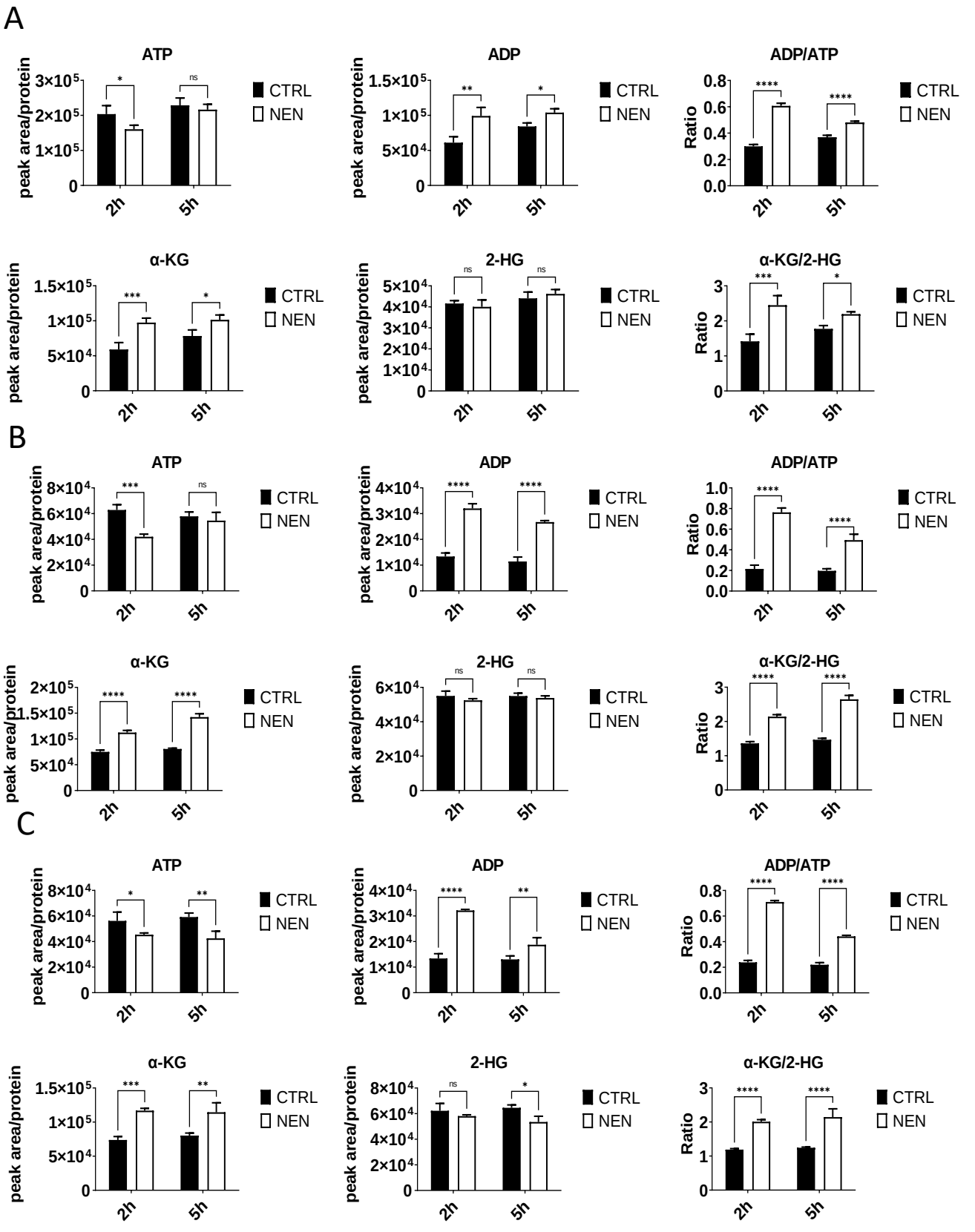

Supplemental Figure 6. The metabolic reprograming effect of NEN on other cancer cell types.
Relative intracellular metabolite levels or ratios were measured using LC-MS in **(A)** Ovcar3 cells, **(B)** H29 and **(C)** H82 cells. Cells were treated with DMSO or 1 μM NEN for 2h or 5h. Data are represent as mean ± SD (n = 3, biologically repeats). Representative of at least two independent experiments. ns: $P > 0.05$, *$P < 0.05$, **$P < 0.01$, ***$P < 0.001$, ****$P < 0.0001$, determined by the Student two-tailed t test.

Supplemental Figure 7

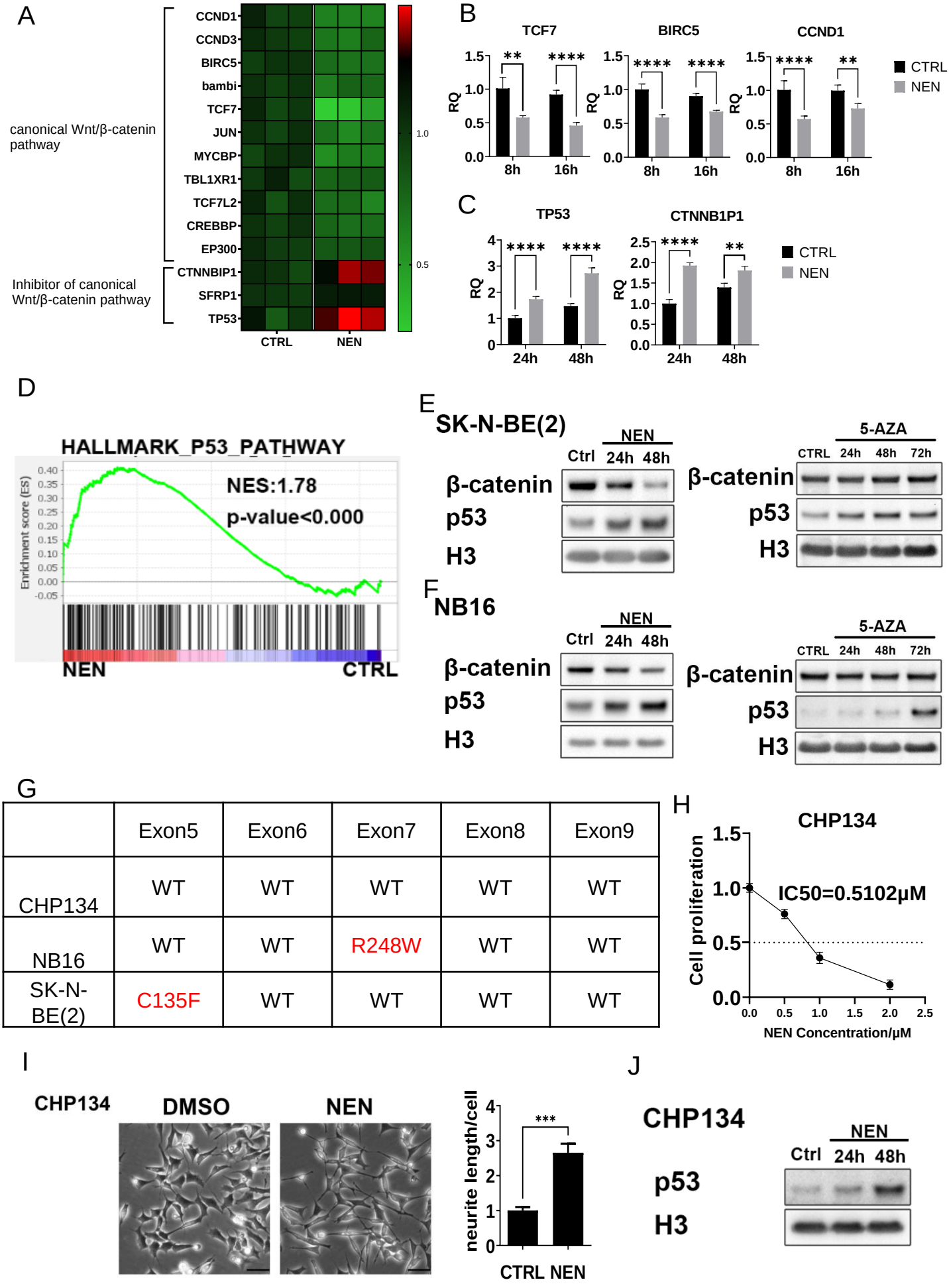

	Exon5	Exon6	Exon7	Exon8	Exon9
CHP134	WT	WT	WT	WT	WT
NB16	WT	WT	R248W	WT	WT
SK-N-BE(2)	C135F	WT	WT	WT	WT

Supplemental Figure 7. Mitochondrial uncoupling upregulates p53 pathway and inhibits the Wnt/β-catenin pathway.

(A) Heat map of Wnt signaling pathway gene expression from the RNA-seq (n=3) experiments in SK-N-BE(2) cells. **(B) (C)** qPCR analysis were employed to validate the RNA-seq data in SK-N-BE(2) cells. **(D)** GSEA of p53 pathway genes from the RNA-seq experiments in SK-N-BE(2) cells. **(E)** SK-N-BE(2) and **(F)** NB16 cells were treated with 1 μM NEN for 24 and 48 hrs (left panel). Or 1 μM 5-AZA for 24 , 48 and 72 hrs (right panel). The protein expression level of β-catenin and p53 of cells were examined using western blot. **(G**) Summary of sequencing results of exon 5, 6, 7, 8 and 9 of *tp53* in CHP134, SK-N-BE(2) and NB16 cells. WT, wildtype. (**H**) CHP134 cells were plated in 12 wells plates ($2x10^4$ cells/well). After 24hrs, cells were treated with DMSO or 1μM NEN for 3 days, and then counted. **(I)** Left: morphological feature of CHP134 treated by DMSO or 1μM NEN for 96h (Scale bar: 50 μM). Right: Quantification of neurite outgrowth with NeuronJ. **(J)** CHP134 cells were treated with DMSO or 1 μM NEN for 24 and 48 hrs. p53 expression was examined using western blot. Data in **(B)** and **(C)** are presented as mean ± SD of three PCR reaction of a representative of two independent experiments. Data in **(E) (F)** and **(H)** are representatives of two independent experiments. *P < 0.05; **P <0.01; ***P < 0.001, ****P < 0.0001 for comparisons were calculated using determined by the Student two-tailed t test.

Supplemental Figure 8

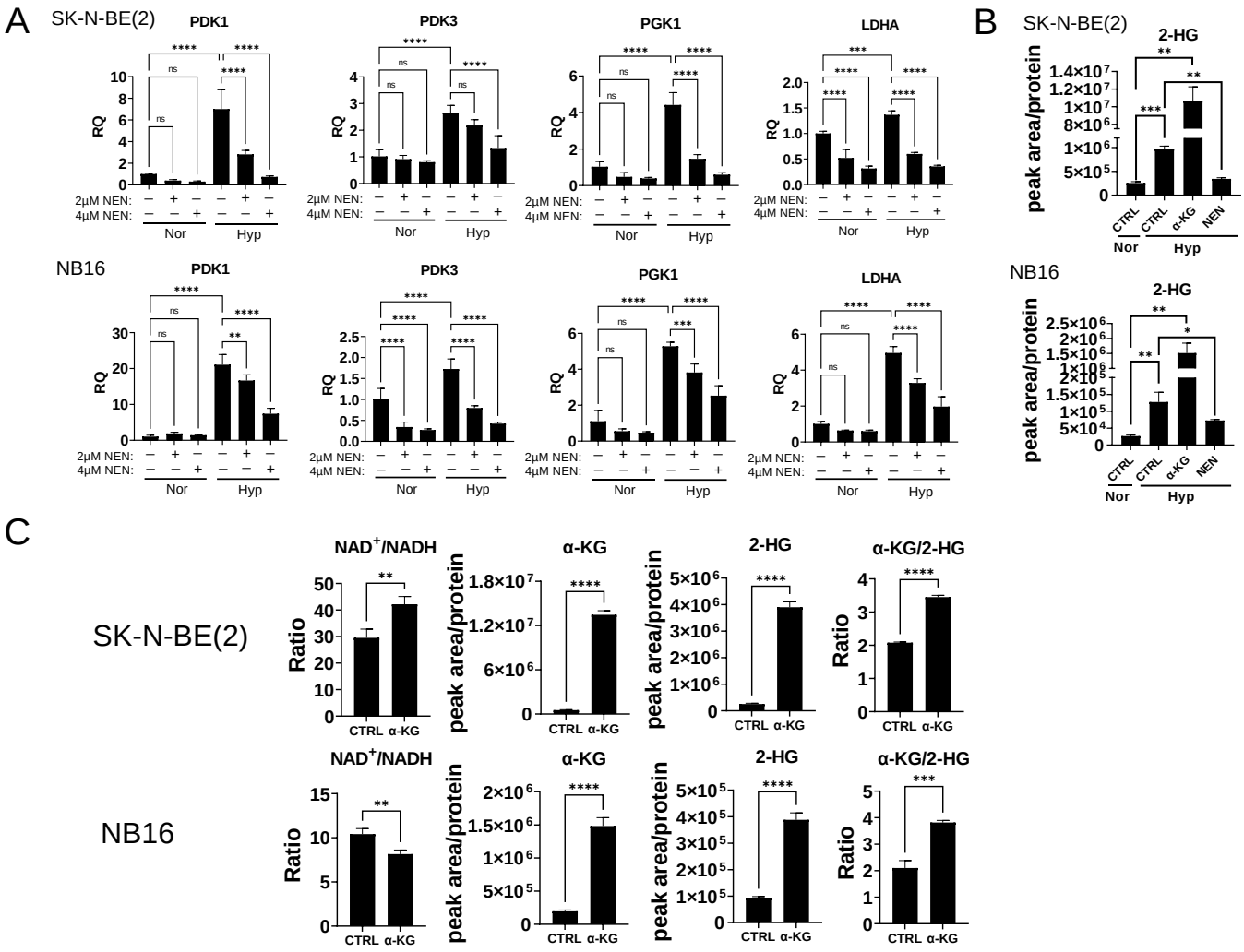

Supplemental Figure 8 NEN inhibited the HIF signaling induced by hypoxia.
(A) Genes expression of HIFs targeted were measured by RT-qPCR in SK-N-BE(2) and NB16 cells treated with DMSO, 2μM NEN, 4μM NEN under normoxia or hypoxia (0.5% oxygen) for 24hrs. **(B)** Intracellular 2-HG were measured by LC-MS in SK-N-BE(2) and NB16 cells treated by DMSO, 3.5mM α-KG or 1 μM NEN under hypoxia (0.5% oxygen) for 16h. **(C)** Relative intracellular metabolites were measured using LC-MS in SK-N-BE(2) and NB16 cells treated with control or 3.5mM Dimethyl 2-oxoglutarate (DMKG) under normoxia for 5h. Data are represented as mean ± SD of three biological repeats. ns: P > 0.05, *P < 0.05 **P < 0.01 and ***P < 0.00, ****P < 0.0001 for comparisons were calculated using one-way ANOVA test or Student's two-tailed t-test. .

Supplemental Figure 9

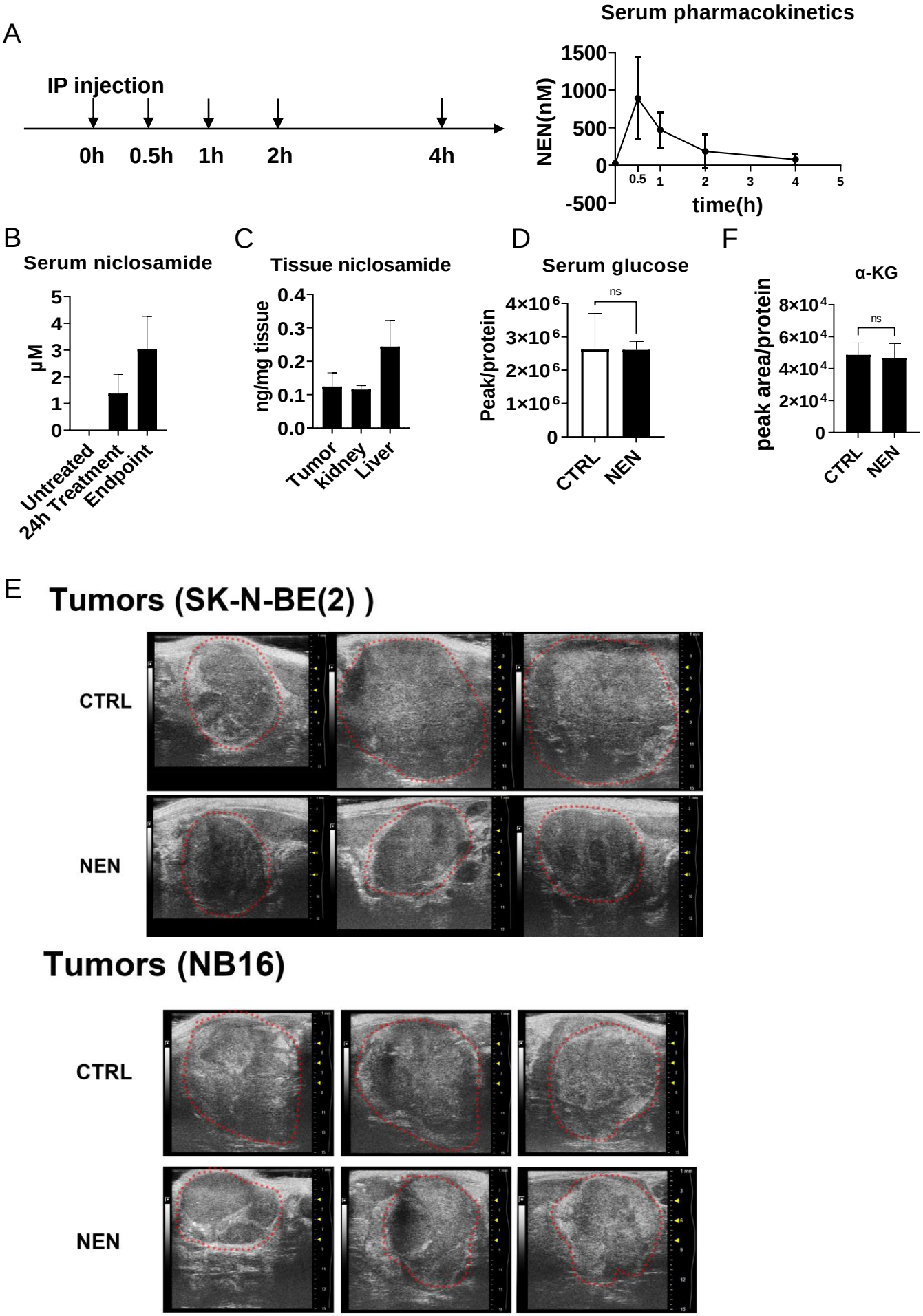

Supplemental Figure 9. Pharmacokinetics of NEN in mice.
(A) 250μg NEN in DMSO were delivered to the mice through intraperitoneal injection. Blood collection were performed for indicated time by tail vein sampling. The niclosamide concentration were measured using LC-MS. **(B)** The serum niclosamide levels were measured using LC-MS in mice fed with NEN diet for indicted time. **(C)** The tissue niclosamide levels were measured using LC-MS in mouse feed with NEN diet at endpoint. **(D)** Relative metabolite levels were measured using LC-MS serum of the mice at the endpoint of the SK-N-BE(2) experiment. **(F)** Relative metabolite levels were measured using LC-MS in tumors (SK-N-BE(2)) (n=5). Data in **(A)** is presented as mean ± SD (n=3). **(E)** Represented ultrasound scanning pictures of tumor after 21 days treatment. Data in **(B) (C) (D)** and **(F)** represent the mean ± SD *P < 0.05, **P < 0.01 and ***P < 0.001, determined by determined by Student's two-tailed t-test.

Supplemental Figure 10

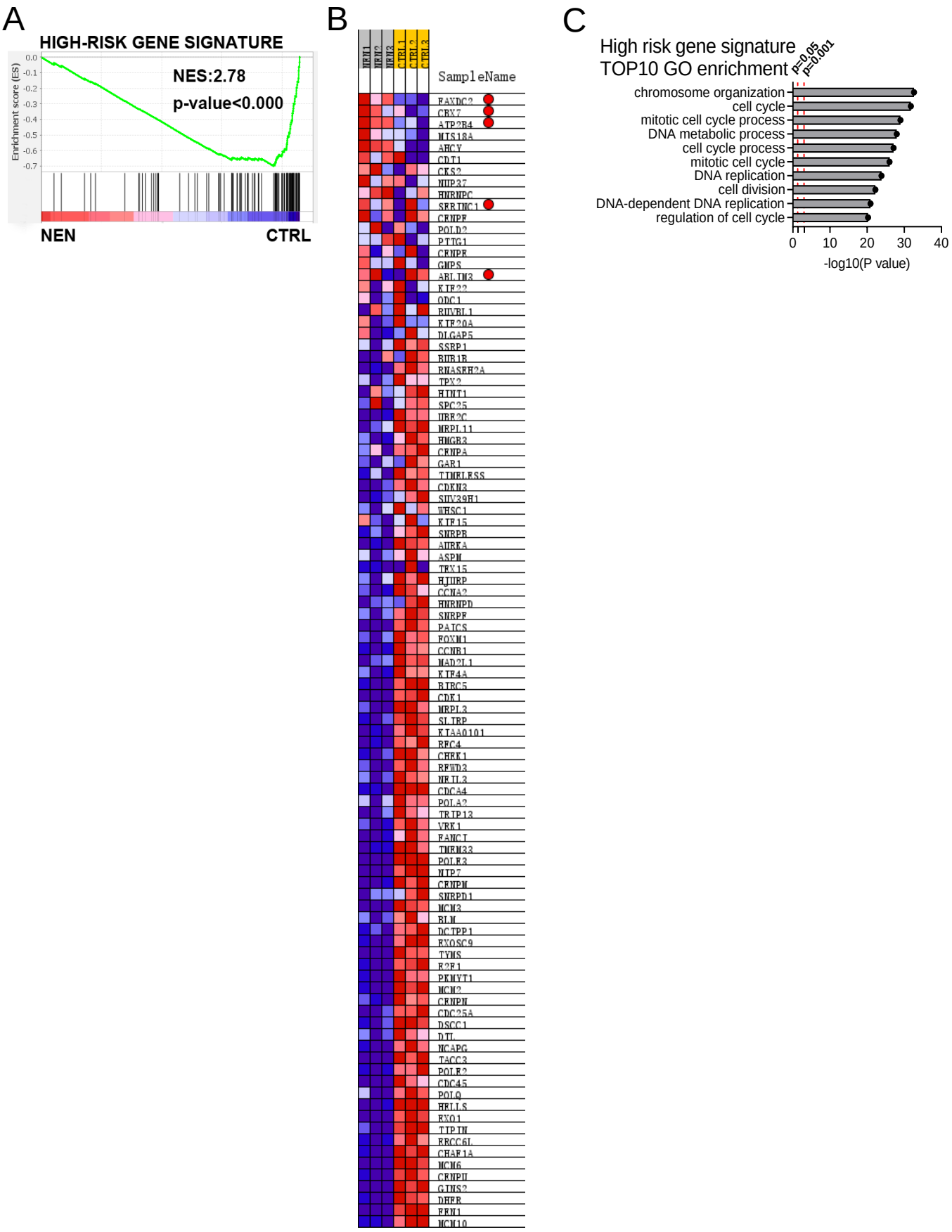

Supplemental Figure 10.
(A) GSEA analysis of high risk gene signature (Clin Cancer Res (2019) 25 (13): 4063–4078.) from RNA-seq experiments in Figure 1 (D). **(B)** The heatmap of the high risk gene signature (n=99) expression changes by NEN treatment. The 5 genes marked with red circle are correlated with favorable prognosis. The rest 94 genes are correlated with unfavorable prognosis. **(C)** The top 10 gene ontology (GO) pathways enrichment of high risk gene signature using DAVID analysis.

Table legends

Table S1 SK-N-BE(2) cells were treated with NEN for 16hrs. **(A)** Upregulated and **(B)** downregulated genes from RNA-seq data (n=3) (sleuth q-value < 0.05 and fold change estimate b > abs(ln(2))). **(C)** The top 10 gene ontology (GO) pathways enriched from upregulated genes by using DAVID analysis. **(D)** The top 10 gene ontology (GO) pathways enriched from downregulated genes by using DAVID analysis.

Table S2 (A) Regional counting of differential methylated probes in SK-N-BE(2) cells treated with NEN for 24hrs under nomoxia. Go enrichment pathways of the differential methylated probes of the CpG Island in the promoter **(B) (C)** and gene body **(D) (E)**.

Table S3 (A) Favorable and **(B)** unfavorable gene list (p-value<0.05) from 11 available neuroblastoma databases from R2 (https://hgserver1.amc.nl/cgi-bin/r2/main.cgi) **(C)** Overlapped the favorable prognosis gene sets (p-value<0.05, gene number >1000) from 7 available neuroblastoma databases from R2 (https://hgserver1.amc.nl/cgi-bin/r2/main.cgi). **(D) (E)** Go analysis of overlapped favorable and unfavorable prognosis gene sets. **(F) (G)** GSEA analysis of Favorable and unfavorable gene list genes from RNA-seq experiments in Figure **(1D).**

Table S4 Primers for p53 mutation analysis.